Structural Engineering and Mechanics, Vol. 25, No. 2 (2007) 131-146
DOI: http://dx.doi.org/10.12989/sem.2007.25.2.131

Modeling and damage detection for cracked I-shaped steel beams

Jun Zhao†

A. Epstein and Sons, Inc., Chicago, IL, USA

John T. DeWolf‡

Department of Civil & Environmental Engineering, University of Connecticut, Storrs, CT, USA

(Received June 3, 2005, Accepted August 25, 2006)

Abstract. This paper presents the results of a study to show how the development of a crack alters the structural behavior of I-shaped steel beams and how this can be used to evaluate nondestructive evaluation techniques. The approach is based on changes in the dynamic behavior. An approximate finite element model for a cracked beam with I-shaped cross-section is developed based on a simplified fracture model. The model is then used to review different damage cases. Damage detection techniques are studied to determine their ability to identify the existence of the crack and to identify its location. The techniques studied are the coordinate modal assurance criterion, the modal flexibility, and the state and the slope arrays.

Keywords: coordinate modal assurance criterion; cracking; damage detection; finite element modeling; modal flexibility; mode shapes; natural frequencies; nondestructive evaluation; state and slope arrays; steel beams.

1. Introduction

In 1988, a crack developed in one of the primary steel I-shaped girders in a multi-girder Rhode Island Bridge ("R.I. Shores" 1988). The crack extended through a depth larger than half of the girder depth. In addition, subsequent inspection showed that a crack was developing in the adjacent girder. Fortunately, a passerby happened to observe light through the crack and reported the problem to the department of transportation. The bridge had been inspected approximately six months earlier, with no sign of the crack. This is an example where nondestructive monitoring as a supplement to visual inspections at the normal two-year cycle would be beneficial.

Researchers at the University of Connecticut have been exploring different approaches to conduct nondestructive monitoring for application to bridges. This paper reports on a study of techniques that can be used for continuous nondestructive evaluation to provide warning of significant cracking, such as occurred in the Rhode Island bridge.

† Structural Engineer, Senior Project Engineer
‡ Professor, Corresponding author, E-mail: dewolf@engr.uconn.edu

When a crack develops in a steel beam, there are changes in the local flexibility at the location of the crack. This results in a small change in the overall structural performance. The change is more readily reflected in the dynamic behavior, than in the static behavior. This is because the dynamic parameters are normally less dependent on the type, location and magnitude of the load than are the static parameters.

This paper reports on the development of an approximate finite element model that can be used to study the dynamic behavior of cracked I-shaped beams. The model is used to explore the vibration behavior and to review nondestructive techniques for damage detection. Different dynamic diagnostic parameters are compared for use in both the detection of structural damage and the location of the crack.

The dynamic behavior of a beam with an edge-crack has been studied by different researchers. Papadopoulos and Dimarogonas (1987) studied the vibration of cracked shafts in bending and the coupling of longitudinal and bending vibrational modes for a rotating shaft with surface cracks. Gounaris and Dimarogonas (1988) studied the response in a prismatic rectangular beam subject to harmonic point force excitation. Using finite element analysis for a rectangular beam, Qian *et al.* (1990) investigated the changes in the natural frequencies and the effect of crack closure as an identification technique in the time domain. Rizos and Aspragathos (1990) identified the crack location and magnitude for a rectangular beam using the measured vibration amplitudes at two points in the beam. The vibrational behavior of a rotor bearing system with a crack was analyzed by Inagaki *et al.* (1982) using an iterative numerical calculation method.

Many who have proposed use of vibrational behavior for damage detection have relied on use of the natural frequencies and/or the mode shapes (Kim and Stubbs 1995, DeWolf *et al.* 1995, Law *et al.* 1995, Alampalli *et al.* 1995, Lauzon and DeWolf 1996, Zhao and DeWolf 1998, 1999). Derivatives of natural frequencies and mode shapes, involving higher order functions have also been used. These include the modal assurance criterion (MAC), the coordinate modal assurance criterion (COMAC) (Alampalli *et al.* 1995, DeWolf and Zhao 1998, Zhao and DeWolf 1999); modal flexibility (Raghavendrachar and Aktan 1992, Shelley 1995, Toksoy and Aktan 1995, Aktan *et al.* 1995, Zhao 1998); and a modified modal flexibility approach (DeWolf and Zhao 1998, Zhao and DeWolf 1999). Stubbs and Garcia (1996) studied plate girders using finite elements to simulate damage. Silva and Gomes (1990) conducted experimental studies of cracked beams with rectangular cross-sections.

In practice, cracks in the flange of the I-shaped steel beam, with or without extension into the web, are propagated by fracture due to stress concentrations at the crack tip. In this study, an approximate finite element model is developed for a plane beam with rectangular cross-section based on consideration of the stress intensity factors and strain energy. The model is then extended to the beams with I-shaped cross-sections. The model for the I-shaped cross-section is then used to study different damage cases. Of interest is the ability to verify that there has been a major crack, as well as the determination of the crack location. The methods studied are the coordinate modal assurance criterion, the modal flexibility, and the state and the slope arrays.

2. Finite element model for rectangular beam

Zhao and DeWolf (1999) explored use of nondestructive evaluation techniques based on vibrations for evaluation of a spring-mass system. The research reported in this paper was carried

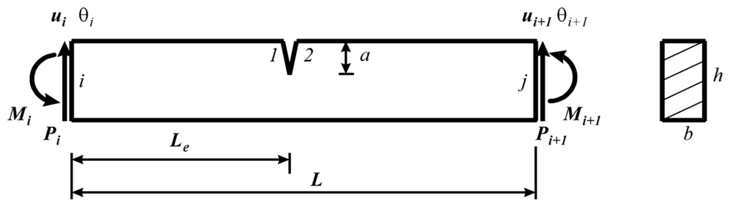

Fig. 1 Beam element with crack

out to develop a finite element model of a beam with a crack that can be used to continue the work conducted with the spring-mass system. This section reports on the development of an approximate finite element model to represent a crack in a I-shaped beam. The goal is to use it to explore nondestructive evaluation techniques. A more complete derivation is given by Zhao (1998).

Derivation - The element stiffness matrix for the cracked beam, shown in Fig. 1, is derived as follows. Using Saint-Venant's principle as an approximation, cracking is assumed to affect the stress field only in the small region near the crack. The beam is then divided into three components, one from left end to node 1, one from node 2 to the right end, and one between nodes 1 and 2. The first and third components are based on the traditional beam elements. Nodes 1 and 2 refer to the cross section location immediately before and after the crack. The first and third components are treated as regular beam elements without cracks, using conventional element stiffness matrices. The stiffness matrix for the interior element containing the crack is derived from the assumed displacements based on the reduction in the stiffness at the crack.

The assumptions for the elements are: (1) prismatic cross-section; (2) elastic behavior; (3) small deformations; (4) constant crack depth. In addition, the possibility of the crack closing is neglected. In the applications of interest in this investigation, the crack forms in the tension zone. As a consequence, the dead load will typically assure that there is continued separation at the crack.

The presence of a transverse crack in the structural member will lead to an increase in the strain energy at the crack tip, with a corresponding increase in the flexibility. A local flexibility matrix was introduced by Papadopoulos and Dimarogonas (1987). The matrix size depends on the number of the degrees of freedom considered, with a maximum dimension equal to 6 by 6. This applies to a spatial structure with a general loading case. There are three translation and three rotational degrees of freedom at each node in the structure. The matrix is based on expressions for the stress intensity factors and the associated expressions for the strain energy density function, as described in the following.

The increase in the displacements u_i of a beam when a crack of depth a develops in the ith direction (Tada 1973) is:

$$u_i = \frac{\partial}{\partial P_i}\left[\int_0^a J(a)da\right] \tag{1}$$

In this equation, $J(a)$ is the strain energy density function and P_i is the corresponding load in the $i$ty direction. The local flexibility coefficients for the general case is defined (Dimarogonas 1983) as:

$$c_{ij} = \frac{\partial u_i}{\partial P_j} = \frac{\partial}{\partial P_i \partial P_j}\left[\int_0^a J(a)da\right] \tag{2}$$

The local flexibility coefficients in Eq. (2) are now used to develop element stiffness matrices for the element with a crack with depth a, located L_e from left end of the beam. Each one of the nodes has two degrees of freedom, one in the translation direction and the other in the rotational direction. These flexibility coefficients can be used to determine flexibility matrix, and this is then converted to the stiffness matrix.

The strain energy density function of a plane beam due to the crack is:

$$J(a) = \frac{(K_{IM})^2 + (K_{IIP})^2}{E'} \tag{3}$$

where (Tada 1973) $K_{IM} = \sigma\sqrt{\pi a}F_I(s); \quad K_{IIP} = \tau\sqrt{\pi a}F_{II}(s);$

$$F_I(s) = \sqrt{\frac{2\tan(\pi s/2)}{\pi s}}\left\{\frac{0.923 + 0.199[1 - \sin(\pi s/2)]^4}{\cos(\pi s/2)}\right\};$$

$$F_{II}(s) = \frac{1.122 - 0.561s + 0.085s^2 + 0.18s^3}{\sqrt{1-s}} \tag{4}$$

where s is the ratio of the crack depth to the beam depth and E' is Young's Modulus of Elasticity.

It can be shown that in Eq. (4) both $F_I(s)$ and $F_{II}(s)$ are approximately 1.122 when the depth of the crack is small. This then results in stress intensity factors that are essentially constant. The constant normal stress, σ, and the constant shear stress, τ, of the beam may be approximated as $\sigma = \frac{6M}{bh^2}$ and $\tau = \frac{P}{bh}$, respectively. The flexibility coefficients due to the crack are then obtained as:

$$c_{22} = \frac{\partial^2 u}{\partial M^2} = \frac{72\pi}{bh^4}\int_0^a a\frac{F_I^2(s)}{E'}da; \quad c_{11} = \frac{\partial^2 u}{\partial P^2} = \frac{2\pi}{bh^2}\int_0^a a\frac{F_{II}^2(s)}{E'}da; \text{ and}$$

$$c_{12} = c_{21} = \frac{\partial^2 u}{\partial M \partial P} = 0.0 \tag{5}$$

where c_{11}, c_{22}, c_{21} and c_{12} represent the flexibility coefficients due to the shear force, the bending moment, and the coupling between bending and shear forces in the beam.

For a prismatic element, the relationship between nodes i and j in the force and the displacement components can be expressed as:

$$\begin{Bmatrix} P_i \\ M_i \\ P_j \\ M_j \end{Bmatrix} = [k]_e \begin{Bmatrix} u_i \\ \theta_i \\ u_j \\ \theta_j \end{Bmatrix} = [K]_e\{\delta\}_e \tag{6}$$

where $[K]_e = \begin{bmatrix} -[T]_{12}^{-1}[T]_{11} & [T]_{12}^{-1} \\ [T]_{21} - [T]_{22}[T]_{12}^{-1}[T]_{11} & [T]_{22}[T]_{12}^{-1} \end{bmatrix}$ is the element stiffness matrix and

$$[T]_{11} = \begin{bmatrix} 1 & (L_{i1} + L_{2j}) \\ 0 & 1 \end{bmatrix}; \quad [T]_{21} = \begin{bmatrix} 0 & 0 \\ 0 & 0 \end{bmatrix}; \quad [T]_{22} = \begin{bmatrix} -1 & 0 \\ (L_{i1} + L_{2j}) & -1 \end{bmatrix};$$

$$[T]_{12} = \begin{bmatrix} \dfrac{L_{i1}L_{2j}(L_{2j} + L_{i1})}{2EI} + \dfrac{(L_{2j}^3 + L_{i1}^3)}{6EI} - c_{11} + c_{22}L_{i1}L_{2j} & -\dfrac{(L_{2j}^2 + L_{i1}^2)}{2EI} - \dfrac{L_{i1}L_{2j}}{EI} - c_{22}L_{i1} \\ \dfrac{(L_{2j}^2 + L_{i1}^2)}{2EI} + c_{22}L_{2j} + \dfrac{L_{i1}L_{2j}}{EI} & -\dfrac{(L_{2j} + L_{i1})}{EI} - c_{22} \end{bmatrix}$$

The stiffness matrix with cracks was verified to be symmetric by Zhao (1998). Zhao also verified that it reduces to the conventional general element stiffness matrix for the case without cracks.

Verification - The finite element analysis (FEA) was verified using a beam with a rectangular cross-section and an edge crack. Two cases were used in the verification, a cantilevered beam with an applied moment and a simply supported beam with shear forces (Zhao 1998). The results were compared with an analytical solution based on the study by Gudmundson (1982). Based on this work, the resulting cracked structural natural frequency can be shown to be:

$$\frac{f_{n,cracked}^2}{f_{n,uncracked}^2} = \left[1 - \frac{W_n'}{W_{n,0}}\right] \tag{7}$$

where f_n is the nth natural frequency of the beam, and W_n' and $W_{n,0}$ are the strain energy of the beam based on nth natural frequency with and without a crack, respectively.

The first comparison (Zhao 1998) was based on the case with constant stress intensity factors in which $F_I(s)$ and $F_{II}(s)$ can be approximated as 1.122, which is correct for small cracks. This value is based on a numerical study, reported in the above reference. The agreement was excellent. For cases in which the variable stress intensity factors $F_I(s)$ and $F_{II}(s)$ are not correctly approximated as 1.122, the results are not as good as the case using constant stress intensity factors. The error becomes significant when the crack is deeper than approximately 20% of the depth of the beam. As noted, this comparison was made for a rectangular cross-section.

3. Finite element model for I-shaped cross-section beam

Derivation - The difference in using the finite element analysis model for an I-shaped beam as opposed to a rectangular beam is in the development of the flexibility coefficients. For an I-shaped cross-section beam, two possibilities are considered in the finite element analysis model. In the first, the crack exists only in the flange, and in the second, the crack extends through the flange into the web. Both are shown in Fig. 2.

When the crack exists only in the flange, the flexibility coefficients are approximately the same as for the rectangular beam. When the crack extends into the web, the crack may be divided into two

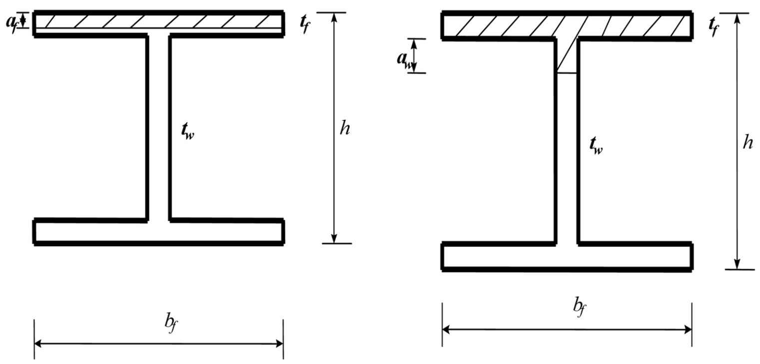

Fig. 2 I-Shaped beam with crack possibilities

parts: the part in the flange and the part in the web. These two parts are treated separately as two rectangular sections. The results are superimposed to obtain the strain energy. The strain energy of the beam may be approximated as:

$$J(a) = b_f \int_0^{t_f} \frac{(K_{IM}^2 + K_{IIP}^2)}{E'} da + t_w \int_0^{a_w} \frac{(K_{IM}^2 + K_{IIP}^2)}{E'} da \tag{8}$$

The flexibility coefficients used in finite element model are then:

$$c_{11} = \frac{3.9549(1-\mu^2)}{ES^2}(b_f t_f^2 + t_w a_w^2), \quad c_{22} = \frac{0.988725(1-\mu^2)h^2}{EI^2}(b_f t_f^2 + t_w a_w^2) \text{ and } c_{12} = c_{21} = 0$$

Verification - A simply supported beam with a crack in the flange only is used first to verify the model. Based on the method for the evaluation of the changes in the natural frequencies due to an edge crack, as presented by Gudmundson (1982), a simple beam with an I-shaped cross-section may be expressed as:

$$\frac{f_{n,cracked}^2}{f_{n,uncracked}^2} = 1 - \frac{7.9098(1-\mu^2)Ia^2}{L\left(1 + \frac{2(1+\mu)In^2\pi^2}{\alpha_r L^2}\right)} \left\{ \frac{h^2}{4I^2} \sin^2\left(\frac{n\pi x}{L}\right) + \frac{n^2\pi^2}{S^2L^2} \cos^2\left(\frac{n\pi x}{L}\right) \right\} \tag{9}$$

where I is the moment of inertia, μ is Poisson's ratio, a is the crack depth, n is the number corresponding to the natural frequency and S_r is the shape factor for shear (1.2 for rectangular sections).

When the crack extends through the flange into the web, the changes in the ratio of the nth natural frequency may be expressed as:

$$\frac{f_{n,cracked}^2}{f_{n,uncracked}^2} = 1 - \frac{7.9098(1-\mu^2)I}{L\left(1 + \frac{2(1+\mu)In^2\pi^2}{\alpha_r L^2}\right)} (b_f t_f^2 + t_w a_w^2) \left\{ \frac{h^2}{4I^2} \sin^2\left(\frac{n\pi x}{L}\right) + \frac{n^2\pi^2}{S^2L^2} \cos^2\left(\frac{n\pi x}{L}\right) \right\} \tag{10}$$

Table 1 Percentage difference in frequency ratio - crack in flange only

Crack depth	Crack location	Percentage difference in frequency ratio as defined by Eq. (9)			
$\frac{a}{t_f}$	$\frac{L_e}{z}$	$\left(\frac{f_{1,cracked}}{f_{1,uncracked}}\right)^2$	$\left(\frac{f_{2,cracked}}{f_{2,uncracked}}\right)^2$	$\left(\frac{f_{3,cracked}}{f_{3,uncracked}}\right)^2$	$\left(\frac{f_{4,cracked}}{f_{4,uncracked}}\right)^2$
0.2	0.1	0.016	0.017	0.036	0.053
0.4	0.1	0.012	0.061	0.148	0.232
0.6	0.1	0.062	0.183	0.381	0.587
0.8	0.1	0.101	0.386	0.782	1.189
1	0.1	0.155	0.703	1.412	2.111
0.2	0.3	0.015	0.075	0.011	0.019
0.4	0.3	0.170	0.325	0.063	0.099
0.6	0.3	0.640	1.006	0.188	0.290
0.8	0.3	1.666	2.319	0.431	0.671
1	0.3	2.980	4.526	0.831	1.319
0.2	0.4	0.234	0.035	0.024	0.070
0.4	0.4	0.252	0.141	0.119	0.359
0.6	0.4	1.058	0.433	0.368	1.077
0.8	0.4	2.566	1.045	0.873	2.487
1	0.4	5.052	2.095	1.750	4.769

In the following, the frequency ratios expressed in Eqs. (9) and (10) are compared with the ratios obtained from finite element model developed in this study. For the I-shaped beams of interest in this investigation, the bending stiffness is primarily a function of the flanges. Once the crack reaches the web so that the full flange thickness is cracked, the loss in the beam stiffness is significant. At this point, further cracking results in little further loss in the stiffness. Thus, the constant stress intensity factors in which F_I(s) and F_{II}(s) can continue to be approximated as 1.122 because the overall crack depth is small relative to the depth of the cross-section. Thus, as an approximation in this development, the value 1.122 is used for F_I(s) and F_{II}(s) in the development of the stiffness matrix for I-shaped cross-sections for all crack depths. In other words, the primary effect from the crack is due to the crack in the flange, located near the edge, not due to cracking in the web.

Crack in flange only - The relative differences in the ratios of the frequency as defined in Eq. (9) when the crack is in the flange only are shown in Table 1. These differences are based the percentage difference in the ratios of the frequencies ($f^2_{n,cracked}/f^2_{n,uncracked}$) between the values obtained from Eq. (9) and those obtained from the finite element analysis model. This table shows that unless the crack extends through the full flange, or nearly through the flange, and it is away from the support, there is only a very small percentage change in the frequency ratio. If the crack extends through 80 percent of the flange and is in the middle half of the beam, there is a 2 percent or greater change in the frequency ratio defined by Eq. (9) for one or both of the first and second modes.

Table 2 Percentage difference of frequency ratio - crack in flange and web

Crack depth	Crack location	Percentage difference in frequency ratio as defined by Eq. (9)			
$\frac{a}{t_f}$	$\frac{L_e}{L}$	$\left(\frac{f_{1,cracked}}{f_{1,uncracked}}\right)^2$	$\left(\frac{f_{2,cracked}}{f_{2,uncracked}}\right)^2$	$\left(\frac{f_{3,cracked}}{f_{3,uncracked}}\right)^2$	$\left(\frac{f_{4,cracked}}{f_{4,uncracked}}\right)^2$
2	0.1	0.010	0.730	1.483	2.224
3	0.1	0.216	0.822	1.666	2.485
4	0.1	0.461	0.981	1.984	2.937
5	0.1	0.182	1.212	2.454	3.599
2	0.3	3.241	4.731	0.873	1.393
3	0.3	3.836	5.374	0.988	1.584
4	0.3	4.646	6.460	1.186	1.919
5	0.3	6.261	8.080	1.473	2.418
2	0.4	5.238	2.198	1.839	5.006
3	0.4	6.215	2.508	2.099	5.639
4	0.4	7.291	3.030	2.545	6.712
5	0.4	9.456	3.819	3.214	8.231

Crack extending into the web - The relative differences in the frequency ratios, as defined by Eq. (9), for cracks that extend into the web are listed in Table 2. This table shows that if the crack is close to the support, it will be necessary to look at the third and fourth modes to see a percentage change above 1 percent, unless the crack extends through approximately half of the web depth. If the crack is at other locations, the percentage differences are much greater, especially for the first and fourth modes, even in the case where the crack has only begun to extend into the web. This may be due to the fact that a crack is divided into two independent parts, with the flexibility coefficients of the two parts superimposed in the determination of the strain energy. This approach is based on use of the normal stress at the extreme fiber and the average shear stress at the crack location. Nevertheless, it is concluded that the finite element analysis model can be applied to I-shaped cross-sections since for most solutions, the relative error between the analytical and calculated solution are within 5.0%.

The results demonstrate that the modified finite element stiffness element for cracked beams with I-shaped cross-sections developed in this investigation may be used to study how the development of cracks influences the overall beam behavior. This is based on the comparisons between the reference material and that based on the finite element model in this investigation for cases with small cracks and the study of I-shaped beams in which the bending stiffness is primarily a function of the flanges. The modified finite element is used in the following to simulate damage for use with structural damage identification techniques based on structural dynamic parameters.

4. Damage detection of cracked beams

The finite element analysis model for a cracked plane beam with an I-shape cross-section and an edge crack is used to stimulate damage states and to review different damage identification techniques.

The basic modal parameters used for damage detection are the natural frequencies and mode shapes. In addition to these traditional parameters, diagnostic parameters may be derived from the mode shapes and frequencies. These include the modal flexibility, coordinate modal assurance criterion, state arrays and slope arrays. The third and fourth are the parameters obtained from the frequencies and/or mode shapes, and are defined in the following. The approaches selected for this study are based on the results of a previous study by Zhao and DeWolf (1999) that evaluated different approaches for damage detection.

Coordinate Modal Assurance Criterion (COMAC) - The COMAC represents the correlation between two measured mode shapes at a specific natural frequency from two different tests. The COMAC considers the values all mode shapes at a specific point on the structure. The COMAC identifies where the mode shapes agree or do not agree, indicating potential damage. The COMAC is defined (Lieven and Ewins 1988) as:

$$COMAC(i) = \frac{\left(\sum_{l=1}^{n} \phi_{Al,i}\,\phi_{Bl,i}\right)^2}{\left(\sum_{l=1}^{n} \phi_{Al,i}^2\right)\left(\sum_{l=1}^{n} \phi_{Bl,i}^2\right)} \tag{11}$$

where $\phi_{Al,i}$ is the ith term of lth mode shape in the A set of mode shapes, $\phi_{Bl,i}$ is the ith term of lth mode shape in the B set of mode shapes, and n is the number of the mode shapes.

Modal flexibility - The modal flexibility is based on both the mode shapes and the frequencies. It is defined as the accumulation of the contributions from the measurable modal vectors and corresponding natural frequencies. The modal flexibility matrix $[F]_{n \bullet m}$ is defined (Hoyos and Aktan 1987) as:

$$[F]_{n \bullet m} = [\phi]^T_{n \bullet m}\left[\frac{1}{\omega^2}\right][\phi]_{n \bullet m} \tag{12}$$

where $[F]_{n \bullet m}$ is the modal flexibility matrix of a structure, $[\phi]$ is an unit-mass scaled mode shape matrix, n is the number of measurement points, m is the number of modes, and $[1/\omega^2]$ is a diagonal matrix of ascending natural frequencies. This definition requires knowledge of the unit-mass scaled mode shape matrix. In many applications, the mass information is not available. In these cases, DeWolf and Zhao (1998) have shown that normalized mode shapes can be used in place of the unit-mass mode shapes.

State Array (ST) - A state array is also based on the mode shapes. It represents the difference in nodal values between two mode shapes and is defined (Zhao and DeWolf 1998) as:

$$V_{ST\,i,j} = S^b_{i,j} - S^d_{i,j} \tag{13}$$

where $V_{ST\,i,j}$ is jth term of ith state array, $S^b_{i,j}$ is jth term of ith mode shape without damage, $S^d_{i,j}$ is jth term of ith mode shape with damage on some members, i is the number of mode shapes, and j is the number of terms in the state array.

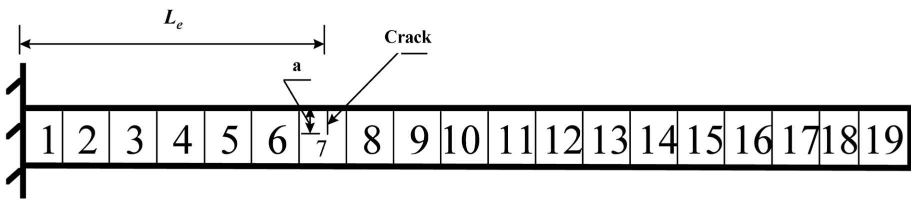

Fig. 3 Cantilever beam with elements

Slope Array (SL) - A slope array is based on the mode shapes. It represents the changes in the slope between two adjacent points in a mode shape and is defined (Zhao and DeWolf 1998) as:

$$V_{SL\ i,j} = (S_{i,j+1} - S_{i,j})/L_{el} \tag{14}$$

where $V_{SL\ i,j}$ is jth term of ith slope array, $S_{i,j+1}$ is $(j+1)$th term of ith mode shape, $S_{i,j}$ is jth term of ith mode shape, L_{el} is the length of elements, i is the number of mode shapes, and j is the number of the terms in the slope array.

Application to beams - The finite element model is now used to study the cantilever beam shown in Fig. 3. The beam has an I-shaped cross-section and a length of L. There is a crack at the top with the depth of a, located L_{el} from the fixed end. The beam is divided into 19 elements. The nodes include the translation and the rotational displacements, so that there are a total of 40 degrees of freedom.

The finite element stiffness matrix derived in this study has been used in a free-vibration analysis to model beams with cracks. The resulting frequencies and mode shapes are used in the following to evaluate their effectiveness for use with different approaches to evaluate changes due to cracking. Also of interest is the ability of these diagnostic parameters to determine the location of the crack. Different damage states are considered, involving both the crack depth and the location. The damage cases are listed in Table 3.

Coordinate Modal Assurance Criterion (COMAC) – Nineteen nodes, from 2 to 20, were used for the calculation of the COMAC, involving either the translation or the rotational displacements. This is based on the assumption that measurement sensors would be used either in the translation

Table 3 Damage cases

Case No.	$\frac{a}{h}$	$\frac{L_{el}}{L}$	Crack locations
1	0.15	0.48	Between 10 & 11, near 10
2	0.15	0.75	Between 14 & 15, near 14
3	0.35	0.22	Between 5 & 6, near 5
4	0.35	0.48	Between 10 & 11, near 10
5	0.35	0.75	Between 14 & 15, near 14

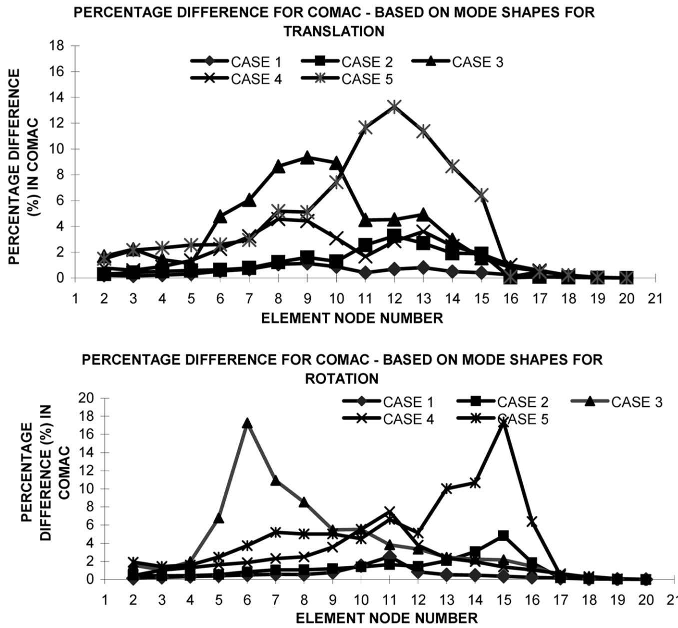

Fig. 4 Results using the coordinate modal assurance criterion

direction or in the rotational direction. It was found that use of the absolute value for each term in the summation of $\phi^T_{Aj,i}\,\phi_{Bk,i}$ in the numerator produces better results than use of normalized mode shapes based on normalization with respect to the maximum absolute modal displacement.

The COMAC was determined using the lowest 5, 10, and 15 mode shapes for the translational and rotational directions. The results are improved when a greater number of mode shapes are used. The results based on use of 15 mode shapes are shown in Fig. 4 for the two separate directions. This figure shows the percentage differences in the COMAC between the uncracked and cracked beams. The larger differences occur for damage cases 3, 4, and 5, those with larger cracks (*a/h* = 0.35). The COMAC based on mode shapes in the rotational direction produced slightly better results. The maximum percentage difference is 13.3% (case 5) based on the mode shapes in translation direction, and it is 17.4% (case 5) based on the mode shapes in rotation direction.

As expected, the COMAC is more successful in identifying cracking than the use of the natural frequencies and mode shapes. The COMAC was also shown to give better results than the Modal Assurance Criterion (Zhao 1998). The plots in Fig. 4 show that the COMAC based on the translation mode shapes indicates damage for damages cases 3, 4 and 5, the cases where the crack has extended through 35 percent of the depth. The translation mode shapes do not correspond to the location of the damage. However, the COMAC based on rotational mode shapes indicates that damage has occurred, and it corresponds to the location of the damage for all but the first damage case.

Modal flexibility - The mode shapes used for the modal flexibility were based on three different comparisons, using mode shapes for: (1) both translation directions or the rotational directions; (2) translation directions only; (3) rotational directions. The results for the first 15 mode shapes are

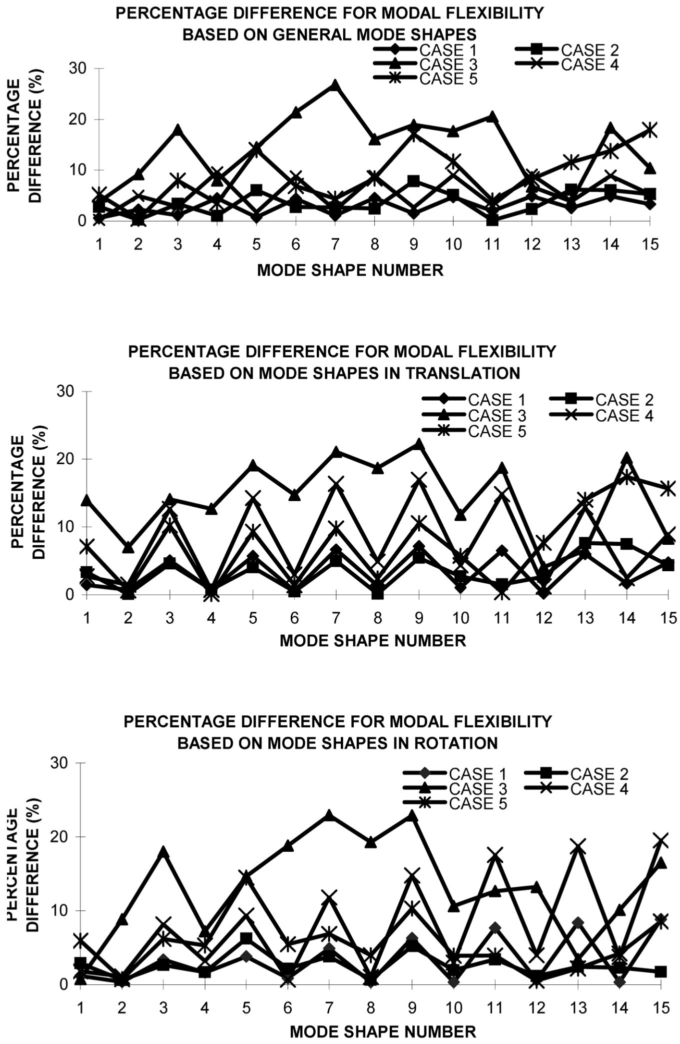

Fig. 5 Results using the modal flexibility approach

shown in Fig. 5 for each of these comparisons, respectively. The maximum percentage differences are substantially larger than those for the COMAC. The damage cases with larger cracks have larger percentage differences. The maximum percentage difference using general mode shapes is 4.9% for case 1, 7.9% for case 2, 26.8% for case 3, 9.6% for case 4, and 17.9% for case 5. The maximum percentage difference using translation mode shapes is 7.1% for case 1, 7.9% for case 2, 22.2% for case 3, 17.0% for case 4, and 17.4% for case 5. The maximum percentage difference using rotation mode shapes is 8.8% for case 1, 6.3% for case 2, 23.0% for case 3, 19.5% for case 4, and 14.6% for case 5. The modal flexibility approach clearly shows when damage has occurred using either the translation or the rotational mode shapes separately, or using both sets together. Unlike the approach based on use of the COMAC, the modal flexibility approach does not indicate the crack location, i.e. peaks in the plots do not generally correspond to crack locations.

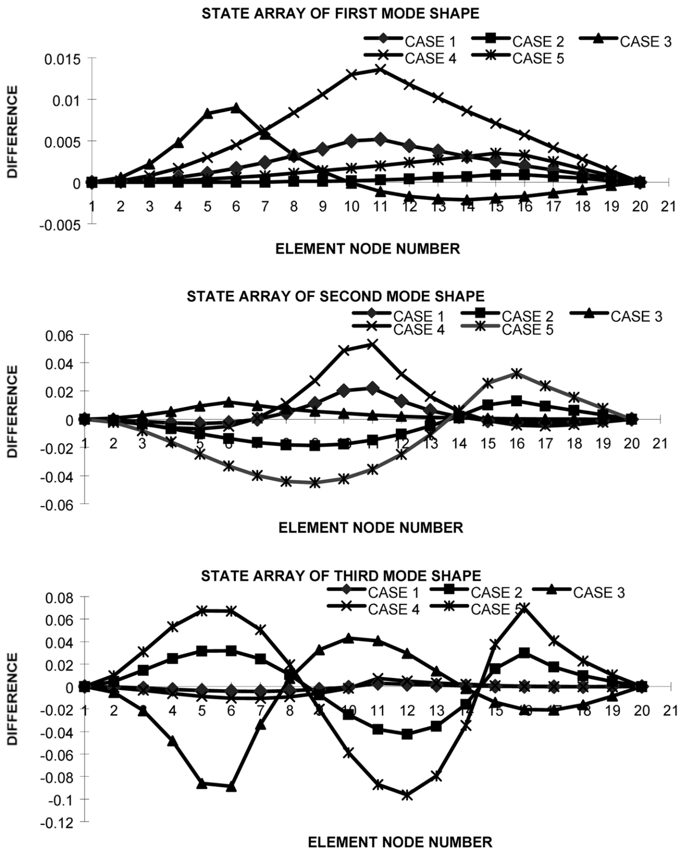

Fig. 6 Results using state arrays

<u>*State Arrays*</u> - The State and Slope Arrays are based on use of normalized translation displacement mode shapes. The difference between the baseline and damaged state arrays in the lowest three translation mode shapes is calculated and plotted in Fig. 6. The state array for the first mode shape produces the greatest values, and thus it provides the best indication that cracking has occurred. There are smaller changes in the second and third state arrays for the second and third mode shapes, though they do show changes as a result of the cracks. In the first mode shape, the peaks in the graphs correspond to the damage location. The second and third mode shapes, while having peaks in the vicinity of the damage, do not appear to be reliable indications of the damage location.

<u>*Slope Array*</u> – Fig. 7 shows the percentage differences for the slope arrays, based on the lowest three mode shapes in the translational direction. The percentages differences for this comparison are much larger than those for the other comparisons. This is consistent with method that is based on using slopes for the mode shapes. A small change in the mode shape displacements will result in a much larger change in the adjacent slopes. Fig. 7 also shows that the higher slope arrays produce larger differences than the lower ones. The figure also shows that the crack locations are not consistently identified for the different damage cases. Nevertheless, while the slope arrays magnify

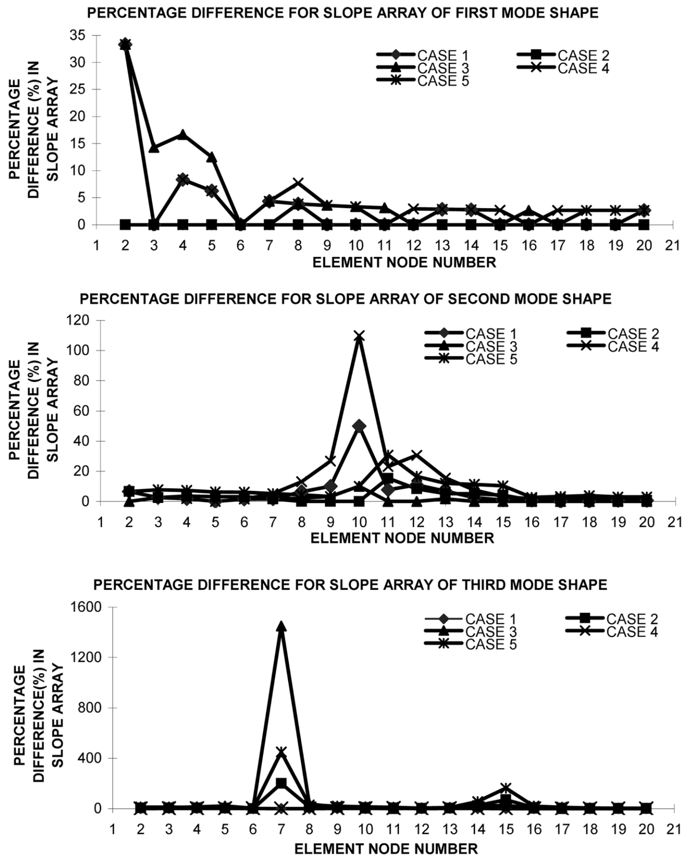

Fig. 7 Results using slope arrays

the changes due to cracking, it is not clear that they would be that useful for monitoring purposes. The authors feel that the variations in the filed data would reduce, or even obscure, the effectiveness of these changes.

The previous theoretical comparisons are based on using up to 15 modes, which is typically more than can be determined in practice. The number of modes available in real applications depends on the resolution of the system used and the amount of noise in the data. The authors do feel that the results can be extended nevertheless to practical applications. This is an area for future study.

5. Conclusions

An approximate finite element model has been developed to study the dynamic behavior of beams with cracks. The beam is modeled with a modified element stiffness matrix based on use of approximate stress intensity factors and a strain energy density function that is based on the crack behavior. The model has been used to review nondestructive evaluation techniques.

Four different damage detection techniques have been explored for a beam in which the crack depths and crack locations are varied. The techniques were evaluated based on how well they were able to determine if the beam had cracked and how successful they were at locating the crack. The main conclusions for each of these methods are:

(1) The coordinate modal assurance criterion magnified the changes due to cracking, indicating that cracking had occurred. It also produced the best estimates for the crack locations.

(2) The modal flexibility method produced consistent indications that there was a crack, with greater magnifications in the data than there are with the coordinate modal assurance criterion. However, it was not successful for locating the crack.

(3) The state arrays, based on comparison of the modal displacements, successfully showed that cracking had occurred. The changes were numerically similar to those from the coordinate modal assurance criterion. The method had mixed results in determining crack locations. The location is clearly shown for the mode shape or shapes that have a peak value in the vicinity of the crack. Unfortunately, this would not work as well in a real application since it would not be clear which mode shape shows the crack location.

(4) The slope array gave the greatest magnification in the variables used to determine if cracking had happened. However, since it is based on slopes of the mode shapes, it is not clear that in actual practice with real numerical data that this method would be successful in showing that cracking has occurred.

In summation, the modal flexibility method gave the best indication that cracking has occurred, assuming that the approach based on the slope array would not be successful in real-life applications. The modal assurance criterion produced the best estimations of the actual crack location.

Acknowledgments

This research is part of a larger study that is developing different techniques for bridge monitoring. It has been supported by the Connecticut Department of Transportation. Their support is gratefully acknowledged.

References

Aktan, A.E., Lee, L. and Dalal, V. (1995), "Multireference modal testing for bridge diagnostics", *North American Workshop on Instrumentation and Vibration Analysis of Highway Bridges*, Cincinnati, Ohio.

Alampalli, S., Fu, G. and Dillon, E.W. (1995), "Measuring bridge vibration for detection of structural damage", Report FHWA/RR-95/165.

Allemang, R.J. and Brown, D.L. (1982), "A correlation coefficient for modal vector analysis", *Proc. of First Int. Modal Analysis Conf.*, Bethel, CT.

DeWolf, J.T., Conn, P.E. and O'Leary, P.N. (1995), "Continuous monitoring of bridge structures", *IABSE Symposium*, San Francisco, CA.

DeWolf, J.T. and Zhao, J. (1998), "Dynamic vibrational techniques in bridge monitoring", Technical Report to Connecticut Department of Transportation, Report CEE-98-1.

Dimarogonas, A.D. and Paipetis, S.A. (1983), *Analytical Methods in Rotor Dynamics*, Applied Science Publishers, London.

Gudmundson, P. (1982), "Eigenfrequency changes of structures due to cracks, notches or other geometrical changes", *J. Mech., Phys., Solids*, **30**(5).

Gudmundson, P. (1983), "The dynamic behavior of slender structures with cross-section cracks", *J. Mech., Phys.,*

Solids, **31**(4).
Hoyos, A. and Aktan, A.E. (1987), “Regional identification of civil engineered structures based on impact induced transient responses”, Res. Report 87-1, Louisiana State Univ., Baton Rouge, LA.
Inagaki, T., Kanki, H. and Shiraki, K. (1982), “Transverse vibrations of a general cracked-rotor bearing system”, *J. of Mech. Design*, **104**.
Kim, J. and Stubbs, N. (1995), “Model-uncertainty impact and damage-detection accuracy in plate girder”, *J. Struct. Eng.*, **121**(10), 1409-1417.
Lauzon, R.G. and DeWolf, J.T. (1996), “Nondestructive evaluation with vibrational analysis”, Nondestructive Testing Methods for Civil Infrastructure, ASCE.
Lauzon, R.G. and DeWolf, J.T. (1993), “Full-scale bridge test to monitor vibrational signatures”, Structural Engineering in Natural Hazards Mitigation, Irvine, CA.
Law, S.S., Ward, H.S., Shi, G.B., Chen R.Z., Waldron, P. and Taylor, C. (1995), “Dynamic assessment of bridge load-carrying capacities”, *J. Struct. Eng.*, **121**(3), 478-487.
Lieven, N.A.J. and Ewins, D.J. (1988), “Spatial correlation of mode shapes, The Coordinate Modal Assurance Criterion (COMAC)”, *Proc. of Sixth Int. Modal Analysis Conf.*, Kissimmee, Florida.
Papadopoulos, C.A. and Dimarogonas, A.D. (1987), “Coupled longitudinal and bending vibrations of a rotating shaft with an open crack”, *J. Sound Vib.*, **117**(1), 81-93.
Papadopoulos, C.A. and Dimarogonas, A.D. (1987), “Coupled of bending and torsional vibration of a cracked Timoshenko shaft”, *Ingenieur Archive,* **57**, 495-505.
Qian, G.L., Gu, S.N. and Jiang, J.S. (1990), “The dynamic behavior and crack detection of a beam with a crack”, *J. Sound Vib.*, **138**(2), 233-243.
Raghavendrachar, M. and Aktan, A.E. (1992), “Flexibility by multireference impact testing for bridge diagnostics”, *J. Struct. Eng.*, **118**(8), 2186-2203.
R.I. Shores Cracked Viaduct (1988), *Engineering News-Record*, McGraw-Hill, Inc. New York, NY, 20-21.
Shelley, S.J. (1995), “Dynamic testing (Vibration Analysis) of highway bridge”, *North American Workshop on Instrumentation and Vibration Analysis of Highway Bridges*, Cincinnati, Ohio.
Silva, J.M. and Gomes, A.J.M. (1990), “Experimental dynamic analysis of cracked free-free beams”, *Experimental Machanics*, **30**, 20-25.
Stubbs, N. and Garcia, G. (1996), “Application of pattern recognition to damage localization”, *Microcomputers in Civil Engineering*, **11**, 395-409.
Tada, H. (1973), *The Stress Analysis of Cracks Handbook*, Del Research Corp., Hellerton, PA.
Toksoy, T. and Aktan, A.E. (1995), “Bridge-condition assessment by modal flexibility”, *North American Workshop on Instrumentation and Vibration Analysis of Highway Bridges*, Cincinnati, Ohio.
Zhao, J. and DeWolf, J.T. (1999), “Sensitivity study for vibrational parameters used in damage detection”, *J. Struct. Eng.*, **125**(4), 410-416.
Zhao, J. (1998), “Nondestructive damage detection using structural dynamic properties”, Thesis of Doctor of Philosophy, University of Connecticut.
Zhao, J., Ivan, J.N. and DeWolf, J.T. (1998), “Structural damage detection using artificial neural networks”, *J. of Infrastructure Systems*, **4**(3), 93-101.